Conformational change in the mitochondrial channel, VDAC, detected by electron cryo-microscopy

Xiao Wei Guo and Carmen A. Mannella

Wadsworth Center for Laboratories and Research, New York State Department of Health, Albany, New York 12201-0509; and Departments of Biomedical Sciences and Physics, The State University of New York at Albany, NY 12203 USA

ABSTRACT   Crystalline arrays of the voltage-dependent channel, VDAC, can be produced by treatment of Neurospora mitochondrial outer membranes with phospholipase A_2. The membrane crystals undergo a lateral phase transition (lattice contraction) that can be induced by an amphipathic polyanion, which also reduces the channel's gating potential. Electron cryo-microscopy of frozen-hydrated crystals indicates that the mean projected diameters of the channels do not decrease with lattice contraction. Instead, contraction is associated with the disappearance of lateral protein "arms" that normally extend between the channels. A model is presented that explains the changes in channel packing and gating potential in terms of a conformational change involving the movement of a protein "arm" between the bilayer and the channel.

INTRODUCTION

Until recently, the mitochondrial outer membrane was considered non-selectively permeable or leaky to all molecules and ions smaller than 5–10 kD. This view is changing with the discovery of several classes of channels in this membrane, each with different permeability properties and voltage dependencies (1–5). The predominant and best characterized of these channels is VDAC (for voltage-dependent, anion-selective channel), also called mitochondrial or eukaryotic porin (1, 6–8). In vitro, this channel has a modest selectivity for anions over cations in its fully open state, and switches to lower conductance substates when 20–30-mV potentials are applied across the membrane. The magnitude of the voltage needed to partially close VDAC (its "gating potential") is greatly reduced by certain macromolecular modulators, which include a synthetic polyanion and an endogenous mitochondrial protein (9, 10). The significance of VDAC's closure has been heightened by recent reports that outer membranes of mitochondria treated with the modulator polyanion are impermeable to ATP (11, 12).

The VDAC channel is formed by a 31-kD polypeptide whose amino-acid sequence is known for several species (13–15). These sequences are characterized by numerous segments of alternating polar/nonpolar residues, suggesting that VDAC's lumen [like that of bacterial porin (16, 17)] may be formed by a cylindrical β-sheet ("β-barrel") with an inner surface lined by polar residues and a hydrophobic outer surface (18, 19). Considerable information about VDAC's structure has come from electron microscopy of two-dimensional crystals of the channel, formed when fungal mitochondrial outer membranes are slowly depleted of lipid by phospholip-

ase A_2 (20, 21). These crystalline arrays are polymorphic, the usually observed oblique array consisting of groups of six channels arranged on a parallelogram lattice with parameters $a = 13.3$ nm, $b = 11.5$ nm, and $\gamma = 109°$. Variants of this lattice geometry are also observed, corresponding to stages of contraction of the parallelogram array (22, 23). The most common contracted array contains the same hexameric group of channels as the oblique array, but arranged on a lattice with smaller angle (100°) and b vector length (10.0 nm).

The polymorphism of crystalline VDAC is interesting, since variations in crystal packing may reflect underlying protein conformational changes. This possibility is especially intriguing in the case of VDAC, since the oblique-to-contracted crystal transition is induced by the modulator polyanion which lowers VDAC's gating potential (24). Thus, determining the nature of structural changes associated with contraction of the VDAC crystal lattice may shed light on the mode of action of this modulator, and possibly on the nature of voltage-induced closure of the VDAC channel.

In the current report, we present evidence from electron cryo-microscopy for a protein conformational change associated with the oblique-to-contracted transition in VDAC crystals.

MATERIALS AND METHODS

Crystalline arrays of the VDAC channel were obtained by treatment of outer membranes isolated from Neurospora crassa mitochondria with phospholipase A_2, as described in detail previously (20, 21). Frozen-hydrated specimens were prepared by depositing 10-μl aliquots of membrane suspension ($\sim$0.2 mg protein per ml of 10 mM Tris-HCl, pH 7.0) on freshly glow-discharged, carbon-coated copper grids, which were then blotted and rapidly plunged into liquid ethane in thermal contact with liquid nitrogen. The frozen-hydrated specimens were transfered to and examined in an EM420-T electron microscope (Philips Electronic Instruments, West Nyack, NY) using a model 626 cryo-transfer device (Gatan, Inc., Warrendale, PA). Images were recorded on Kodak SO163 film (Eastman Kodak Co., Rochester, NY) at 100 kV accelerating voltage and 36,000X magnification using doses of ca. 20 electrons/A^2 and defocus of -250 to -500 nm. Micrographs were
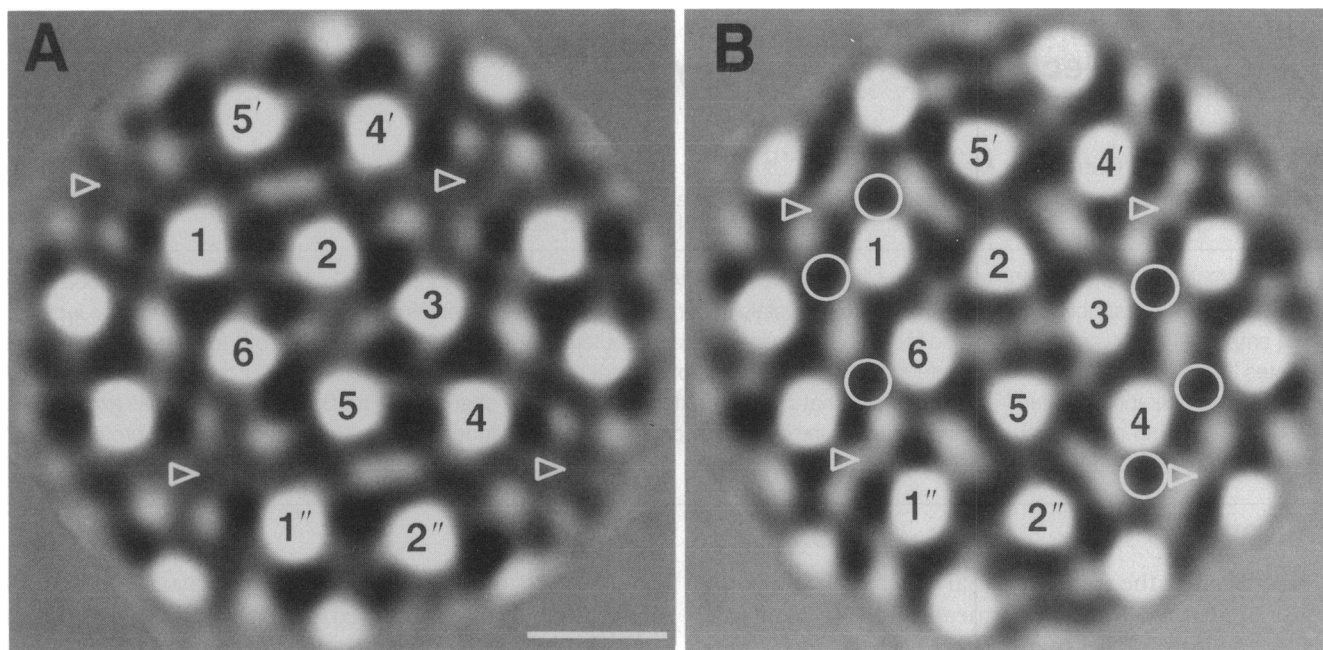
FIGURE 1 Projected density maps of *oblique* (*A*) and *contracted* (*B*) forms of two-dimensional crystals of the VDAC channel, obtained from electron microscopic images of frozen-hydrated crystals. Each map is a representative correlation average including over 300 unit cells from a single membrane crystal, with p2 symmetry imposed. The six channels in the central unit cell of both arrays are numbered, as are the two nearest channels in the adjacent unit cell above (*prime*) and below (*double prime*) the central unit cell. Note the movement of channels 5' and 4' relative to channels 1 and 2, and of channels 1″ and 2″ relative to channels 5 and 4 in the transition from *oblique* (*A*) to *contracted* (*B*) array geometry. The four corners of the *oblique* array (*A*) occupied by lateral protein arms are indicated by arrows, as are the equivalent positions in the *contracted* array (*B*). Sites of increased density on the periphery of the central unit cell in the *contracted* array, which may correspond to redistribution of the mass associated with the arms, are circled in (*B*). Scale bar in (*A*) equals 5 nm.

digitized (0.47 nm per pixel) with a scanning microdensitometer (model PDS 1010A, Perkin-Elmer Corp., Garden Grove, CA) and computer processing was done with the SPIDER system (25), installed on a VAXstation 3500 graphics workstation (Digital Equipment Corp., Maynard, MA). Averages of images of VDAC crystals (which usually consist of collapsed vesicles with two overlapping membrane layers) were obtained by correlation analysis (26, 27), using a procedure described in detail elsewhere (21, 28). Briefly, a subfield (128 × 128 pixels) in a membrane crystal is Fourier-transformed and the inverse transform is computed using only the coefficients corresponding to one of the two overlapped lattices, yielding a preliminary average of one crystal layer. (The procedure may be applied only when the vertices of the two reciprocal lattices do not overlap anywhere in Fourier space.) A reference composed of 5–9 unit cells is windowed from the Fourier-averaged image and cross-correlated with the entire crystal field. The final "correlation average" is computed by summation of subfields windowed from the crystal at the precise positions of maxima in the cross-correlation function (21, 28).

RESULTS AND DISCUSSION

Representative projection images of frozen-hydrated crystalline VDAC, obtained by correlation averaging of images of *oblique* and *contracted* membrane arrays, are presented in Fig. 1. Although resolution (defined in terms of included Fourier components with intensities significantly above background) in correlation averages of *oblique* arrays may extend out to $1/(1.1$ nm$)(29)$, the

average in Fig. 1 *A* has been low-pass filtered at $1/(1.8$ nm$)$. This corresponds to the best resolution so far attainable with correlation averages of *contracted* arrays, like that of Fig. 1 *B*. Since there is no heavy-metal stain present in the specimens, the correlation averages of Fig. 1 correspond to maps of the projected density of the components of the arrays (protein, lipid, water), with white representing low density and black high density. Each channel has a white (water-filled) internal lumen surrounded by a dark (protein) rim, which in turn is bounded by low-density (lipid) domains.

Mean projected diameters of pores in different crystal polymorphs

The channel lumens in the correlation averages of *oblique* and *contracted* arrays (Fig. 1 *A* and *B*) appear to be similar in size. Quantitative comparisons were made of the mean projected lumen diameters in the two types of arrays by a modeling approach used previously for an *oblique* array (29). The projected density at each channel position in the arrays is represented as a circular ring (the axial projection of a hollow cylinder) with a thickness of 0.3 nm and a diameter *D*. Agreement between models of varying ring diameter and projection images of frozen-hydrated VDAC arrays is assessed by the differential phase residual (29, 30):

TABLE 1 Differential phase residuals ($\Delta\phi$) between correlation averages of frozen-hydrated arrays and models of varying lumen diameter (D)

Array image	$\Delta\phi_{min}$*	D_{min}‡	D_{upper}§	D_{lower}‖
	°	nm	nm	nm
Oblique				
#1	33.8	3.7	4.0	3.6
#2	33.0	3.9	4.2	3.6
#3	36.2	3.8	4.0	3.6
#4	43.4	4.0	4.2	3.9
Contracted				
#1	37.7	3.6	3.9	3.4
#2	33.7	3.8	4.0	3.4

* $\Delta\phi_{min}$ = minimum cumulative $\Delta\phi$ over the Fourier annulus $1/(5.0$ nm) to $1/(1.8$ nm).
‡ D_{min} = model ring diameter corresponding to $\Delta\phi_{min}$.
§ D_{upper} = upper limit of model ring diameter for which $\Delta\phi < 45°$.
‖ D_{lower} = lower limit of model ring diameter for which $\Delta\phi < 45°$.

$$\Delta\phi = \left\{ \frac{\Sigma_R(|M_1| + |M_2|)(\Delta\theta)^2}{\Sigma_R(|M_1| + |M_2|)} \right\}^{1/2}$$

where $\Delta\theta$ is the phase difference between the complex Fourier coefficients of the model, M_1, and those of the correlation average, M_2; the summations are made over an annulus, R, in Fourier space. Phase residuals between models of varying ring diameter and images of several *oblique* and *contracted* arrays are summarized in Table 1. The projected diameters of the channel lumens in the two types of arrays are indistinguishable by this method, i.e., both *oblique* and *contracted* density maps are fit best by ring models with diameters in the range 3.6–4.0 nm. Assuming that the channel lumen is formed by a β-barrel aligned normal to the membrane plane, as has been suggested (18, 19), this diameter would correspond to that of the axial projection of the C_α backbone.

The fact that the mean projected lumen diameter of the VDAC channel does not decrease detectably with lattice contraction argues against the contracted lattice representing a closed state of VDAC. However, information about the three-dimensional shape of the pore lumens in both *oblique* and *contracted* arrays is needed to rule out this possibility unambiguously (work in progress).

Structural changes involving the lateral protein arms

Although there is no detectable difference in projected lumen diameters of the channels in the two types of VDAC array, other aspects of the density maps of Fig. 1 *A* and *B* are dissimilar. In particular, the large pore-free areas at the corners of the unit cell in the *oblique* array decrease in area from approximately 17 to 5 nm² in the course of lattice contraction. It is this change in packing

geometry (and not a change in the projected shape of the pore lumen) that accounts for the overall contraction of the surface area of the array by about 10%.

Several dark (protein), lateral features extend from the channels into the corner regions of the unit cell in the *oblique* array, as described previously (29). These protein "arms" are missing from the equivalent regions of the *contracted* array. This local difference in protein arrangement likely reflects a conformational change in the 31-kD VDAC polypeptide, since there is no other protein present in these membrane fractions at sufficient stoichiometry to otherwise account for such a change in crystallographic repeating unit (20). Detailed comparison of the maps of Fig. 1 *A* and *B* reveal several other changes in density distribution that might correspond to rearrangement of the mass associated with the arms after contraction (see legend, Fig. 1). However, it is also possible that some or all of the arms no longer occupy fixed sites in the crystal lattice following contraction, and so disappear upon averaging.

We had previously proposed (29) that the dense lateral arms observed in images of frozen-hydrated *oblique* arrays represent one or more regions of the VDAC polypeptide that extend into lipid domains located at the corners of the unit cell. The results presented in this report are the first direct demonstration that these arms disappear when the lattices contract. It is possible that interaction of these arms at the bilayer surface might stabilize the *oblique* crystal polymorph by preventing the channel hexamers from packing more closely together. Conversely, displacement of the arms from the membrane surface could be a prerequisite for lattice contraction, which would also require removal of lipid from the corner regions of the arrays. This putative movement of an arm of the VDAC polypeptide off the bilayer surface might also have a functional significance, as suggested by the fact that lattice contraction is induced by the synthetic polyanion which lowers VDAC's gating voltage (24). For example, it may be that VDAC's conformation in the *oblique* array represents a low-energy "open" state, stabilized in part by interaction of the extended arms with each other and/or with the surrounding phospholipid (Fig. 2). If so, conditions that weaken these protein–protein and/or protein–lipid interactions would destabilize this "open" state and so lower VDAC's gating potential—and at the same time induce (or at least permit) lattice contraction.

The modulator polyanion which induces contraction of the VDAC crystal lattice is amphipathic, a copolymer of maleate, methacrylate, and styrene. Another molecule also has been shown to exert a similar effect on VDAC arrays, a synthetic peptide with the sequence of the NH_2-terminal targeting region of subunit IV of cytochrome oxidase (31). Although this peptide is a cation and not an anion, it is amphipathic like the modulator polyanion. The amphipathicity of the two contraction-
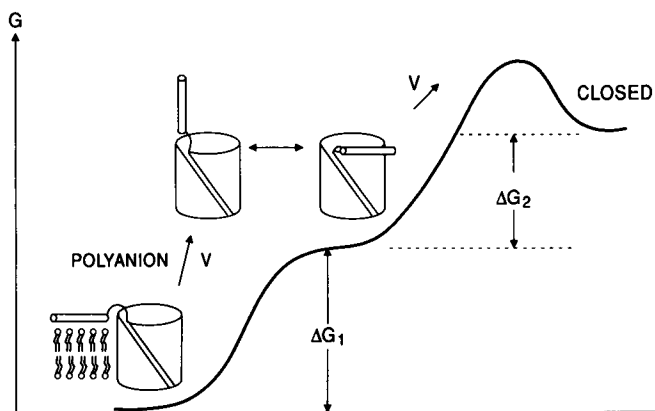
G

FIGURE 2   Hypothetical scheme to explain lattice contraction and decrease in gating potential. The VDAC channel is represented as a β-barrel to which an "arm" is attached by a flexible hinge (see reference 31). The "arms" may normally extend into the adjacent bilayer, stabilizing VDAC's "open" state and preventing the channels from packing closely together. Detachment of the "arms" from the bilayer destabilizes the "open" state (raising its free energy by an amount ΔG_1) and also allows the channels to pack more closely (contracting the crystal lattice). Once detached from the bilayer, the "arms" are free to interact with the channel protein, which may play in a role in subsequent voltage-induced closure. The "gating potential" V_o, defined as the transmembrane voltage for which an equal number of channels are in the "open" and "closed" states, is given by $\Delta G/nF$, where ΔG is the free energy difference between the two states, n is the number of charges involved in the gating process, and F is the Faraday constant. In the "arms extended" conformation, $V_o = (\Delta G_1 + \Delta G_2)/nF$, while in the "arms detached" state, $V_o = \Delta G_2/nF$.

inducing polymers may allow them to insert into phospholipid regions of the crystals and displace VDAC's arm. In fact, the targeting peptide has been shown by electron microscopy to bind to the region in the VDAC crystal occupied by the arms (32). Unfortunately, it is not known at this time whether the targeting peptide alters VDAC's gating characteristics. Determining whether there is a general correlation between the abilities of polymers to alter VDAC's gating potential and to cause crystal lattice contraction may provide important information about the mechanism by which this channel is regulated.

REFERENCES

1. Colombini, M. 1979. A candidate for the permeability pathway of the outer mitochondrial membrane. Nature (Lond.). 279:643–645.

2. Kinnally, K. W., H. T. Tedeschi, and C. A. Mannella. 1987. Evidence for a novel voltage-activated channel in the outer mito-chondrial membrane. FEBS (Fed. Eur. Biochem. Soc.) Lett. 226:83–87.

3. Dihanich, M., A. Schmid, W. Oppliger, and R. Benz. 1989. Identification of a new pore in the mitochondrial outer membrane of a porin-deficient yeast mutant. Eur. J. Biochem. 181:703–708.

4. Chich, J.-F., D. Goldshmidt, M. Thieffry, and J.-P. Henry. 1991. A peptide-sensitive channel of large conductance is localized on mitochondrial outer membrane. Eur. J. Biochem. 196:29–35.

5. Benz, R., A. Schmid, and J. E. Schultz. 1990. Paramecium mitochondria contain three different outer membrane channels. Biophys. J. 57:390a.

6. Zalman, L. S., H. Nikaido, and Y. Kagawa. 1980. Mitochondrial outer membrane contains a protein producing nonspecific diffusion pores. J. Biol. Chem. 255:1771–1774.

7. Freitag, H., W. Neupert, and R. Benz. 1982. Purification and characterization of a pore protein of the outer mitochondrial membrane from Neurospora crassa. Eur. J. Biochem. 123:629–639.

8. Linden, M., P. Gellerfors, and B. D. Nelson. 1982. Purification of a protein having pore forming activity from the rat liver mitochondrial outer membrane. Biochem. J. 208:77–82.

9. Colombini, M., C. L. Yeung, J. Tung, and T. König. 1987. The mitochondrial outer membrane channel, VDAC, is regulated by a synthetic polyanion. Biochim. Biophys. Acta. 905:279–286.

10. Holden, M. J., and M. Colombini. 1988. The mitochondrial outer membrane channel, VDAC, is modulated by a soluble protein. FEBS (Fed. Eur. Biochem. Soc.) Lett. 241:105–109.

11. Benz, R., L. Wojtczak, W. Bosch, and D. Brdiczka. 1988. Inhibition of adenine nucleotide transport through the mitochondrial porin by a synthetic polyanion. FEBS (Fed. Eur. Biochem. Soc.) Lett. 231:75–80.

12. Liu, M. Y., and M. Colombini. 1992. Regulation of mitochondrial respiration by controlling the permeability of the outer membrane through the mitochondrial channel, VDAC. Biochim. Biophys. Acta. 1098:255–260.

13. Mihara, K., and R. Sato. 1985. Molecular cloning and sequencing of cDNA for yeast porin, an outer mitochondrial membrane protein: a search for targeting signal in the primary structure. EMBO (Eur. Mol. Biol. Organ.) J. 4:769–774.

14. Kleene, R., N. Pfanner, R. Pfaller et al. 1987. Mitochondrial porin of Neurospora crassa: cDNA cloning, in vitro expression and import into mitochondria. EMBO (Eur. Mol. Biol. Organ.) J. 6:2627–2633.

15. Kayser, H., H. D. Kratzin, F. P. Thinnes, et al. 1989. To the knowledge of human porins. II. Characterization and primary structure of a 31-kDa porin from human B-lymphocytes (Porin 31HL). Biol. Chem. Hoppe-Seyler 370:1265–1278.

16. Jap, B. K., P. J. Walian, and K. Gehring. 1991. Structural architecture of an outer membrane channel as determined by electron crystallography. Nature (Lond.). 350:167–170.

17. Weiss, M. S., A. Kreusch, E. Schiltz et al. 1991. The structure of porin from Rhodobacter capsulata at 1.8 Å resolution. FEBS (Fed. Eur. Biochem. Soc.) Lett. 280:379–382.

18. Forte, M., H. R. Guy, and C. A. Mannella. 1987. Molecular genetics of the VDAC ion channel: structural model and sequence analysis. J. Bioenerg. Biomembr. 19:341–350.

19. Blachly-Dyson, E., S. Z. Peng, M. Colombini, and M. Forte. 1990. Selectivity changes in site-directed mutants of the VDAC ion channel: structural implications. Science (Wash. DC). 247:1233–1236.

20. Mannella, C. A. 1984. Phospholipase-induced crystallization of channels in mitochondrial outer membranes. Science (Wash. DC). 224:165–166.

21. Mannella, C. A., A. Ribeiro, and J. Frank, 1986. Structure of the

channels in the outer mitochondrial membrane. *Biophys. J.* 49:307–318.

22. Mannella, C. A., M. Colombini, and J. Frank, 1983. Structural and functional evidence for multiple channel complexes in the outer membrane of *Neurospora crassa* mitochondria. *Proc. Natl. Acad. Sci. USA.* 80:2243–2247.

23. Guo, X. W. 1991. Electron microscopic studies of 2D membrane crystals of mitochondrial channel, VDAC, Ph.D. thesis. State University of New York at Albany.

24. Mannella, C. A., and X. W. Guo. 1990. Interaction between the VDAC channel and a polyanionic effector. An electron microscopic study. *Biophys. J.* 57:23–31.

25. Frank, J., B. Shimkin, and H. Dowse. 1981. Spider-a modular software system for electron image processing. *Ultramicroscopy.* 6:343–358.

26. Saxton, W. O. 1980. Matching and averaging over fragmented lattices. *In* Electron Microscopy at Molecular Dimensions. W. Baumeister and W. Vogell, editors. Springer-Verlag GmbH and Co., KG, Berlin. 244–255.

27. Frank, J. 1982. New methods for averaging non-periodic objects and distorted crystals in biologic electron microscopy. *Optik.* 63:67–89.

28. Kessel, M., M. Radermacher, and Frank, J. 1984. The structure of the stalk surface layer of a brine pond microorganism: correlation averaging applied to a double layered structure. *J. Microsc. (Oxf.).* 139:63–74.

29. Mannella, C. A., X. W. Guo, and B. Cognon. 1989. Diameter of the mitochondrial outer membrane channel: evidence from electron microscopy of frozen-hydrated membrane crystals. *FEBS (Fed. Eur. Biochem. Soc.) Lett.* 253:231–234.

30. Frank, J., A. Verschoor, and M. Boublik. 1981. Computer averaging of electron micrographs of 40S ribosomal subunits. *Science (Wash. DC).* 214:1353–1355.

31. Mannella, C. A. 1990. Structural analysis of mitochondrial pores. *Experientia.* 46:137–145.

32. Mannella, C. A., X. W. Guo, and J. Dias. 1992. Binding of a synthetic targeting peptide to a mitochondrial channel protein. *J. Bioenerg. Biomembr.* 24:55–61.